Two-Stage Synthetic Optimization of Supercapacitor-Based Energy Storage Systems, Traction Power Parameters and Train Operation in Urban Rail Transit

Feiqin Zhu, *Student Member, IEEE*, Zhongping Yang, *Member, IEEE*, Ziwei Zhao, and Fei Lin, *Member, IEEE*

***Abstract*—The stationary supercapacitor energy storage system (SCESS) is one of effective approaches for the utilization of train's regenerative braking energy in urban rail systems. In this paper, the capacity configuration of SCESSs, the no-load voltage of substation, the control of onboard braking resistors and train operation diagrams are considered comprehensively. Based on the equivalent circuit model, the effects of traction power system parameters on the energy transmission between powering trains, braking trains and SCESSs are analyzed, and the relationships between the train operating parameters and system energy consumptions are revealed. A multi-variable synthetic optimization method is proposed to optimize the SCESS capacity, train operation diagrams and traction power system parameters collaboratively. In order to reduce the search space and improve the efficiency of the optimization algorithm, a hierarchical multi-objective optimization model is established, based on which the design variables and the control variables are optimized iteratively. And as the traffic density has a great impact on the regenerative braking energy distribution of the system, the optimization objective function fully considers the frequency distribution of headways throughout the day. Combined the Elitist Non-dominated Sorting Genetic Algorithm (NSGA-II) with the traction power flow simulator, the flowchart of the two-stage optimization algorithm is designed, and the pareto set of the multi-objective problem is obtained. The advantages of reducing system energy consumptions and configuration cost under the proposed algorithm are verified based on case studies of Beijing Batong Line.**

***Index Terms*—Energy storage system, train operation, synthetic optimization, regenerative energy, urban rail transit.**

I. Introduction

With the rapid development of urban rail transit, reduction of operation energy consumptions has attracted more and more attention. At present, regenerative braking is widely used for urban railway trains: when the train brakes, the motor converts mechanical energy into electrical energy and feeds it back to the traction network. The regenerative braking energy is considerable due to frequent starts and stops of trains. In recent years, different types of energy storage systems (ESSs), including battery, supercapacitor (SC), flywheel, etc. are applied in urban rail systems to recover the regenerative energy, as well as to stabilize the network voltage and provide emergency power supply [1]. In comparison with other energy storage elements, SC has the advantages of high power density and long cycle life due to its electrostatic storage mechanism, thus copes well with the high and frequent braking power of trains, and achieves good energy-saving effects in a number of metro lines around the world [1]–[3].

A. Literature Review

The siting and capacity configuration are important aspects for the design of ESSs, which a large number of literatures have researched on [4]–[8]. In [5], the capacity allocation is determined by predicting the instantaneous regenerative energy of each station before SCESS installation. However, it does not consider the influence of SCESS power limitation on the energy flow of the system, and doesn't balance the configuration cost and energy-saving effect on the premise that the regenerative energy is fully-recovered. In [6], [7], the relationships between energy-saving effect and capacity configuration of SCESSs at different headways are analyzed based on the assumption that the ESS capacity at each station is the same. In fact, the line conditions, such as slope and station distance differ for substations along the metro line, so the optimal capacity for each station is also distinct. In [8], the improved genetic algorithm (GA) is adopted to optimize the ESS capacity configuration for a typical metro line, and results show that the number of substations where SCESSs should be installed is decreased, as a result of which the investment cost is reduced effectively. In [9], Chaoxian Wu *et al.* employed the mixed-integral linear programming (MILP) model to address the optimal sizing problem of onboard ESSs, and three types of ESSs, including SCs, Li-ion batteries and flywheels are compared in the case of Beijing Changping Line. However, the optimization model does not allow the feedback of regenerative braking energy. In [10], Giuseppe Graber *et al.* proposed a techno-economic method based on particle swarm optimization (PSO) to minimize the annual cost of energy for the

Manuscript received October 13, 2020; revised February 10, 2021 and May 30, 2021; accepted July 11, 2021. Date of publication July 27, 2021; date of current version September 17, 2021. The review of this article was coordinated by Zhigang Liu. *(Corresponding author: Feiqin Zhu.)*

Feiqin Zhu is with the School of Vehicle and Mobility, Tsinghua University, Beijing 100084, China (e-mail: fqzhu@tsinghua.edu.cn).

Zhongping Yang, Ziwei Zhao, and Fei Lin are with the Department of Electrical Engineering, Beijing Jiaotong University, Beijing 100044, China (e-mail: zhpyang@bjtu.edu.cn; 19121542@bjtu.edu.cn; flin@bjtu.edu.cn).

Digital Object Identifier 10.1109/TVT.2021.3100412

auxiliary-battery-based substations (ABS), where the ESSs are equipped to enhance the conventional railway feeder systems. The SC and battery hybrid energy storage systems (HESSs) were also investigated by researchers in the past years [11]–[13]. For example, Victor Isaac Herrera *et al.* proposed a multi-objective optimization method for a battery-SC-based light rail vehicle considering both catenary support and autonomous operation modes [11]. However, the determination of weighting factors was not discussed.

It's also observed from above literatures that only the parameters of ESSs are optimized in most of current researches. As a matter of fact, energy interaction in traction power system is influenced simultaneously by the parameters of trains, substations and ESSs. The improvement of energy-saving effect should also be considered from the systematic perspective [14]–[16]. The train driving strategy affects the operation energy consumption of single train, and the multi-train distribution influences the energy interaction between trains as well as the feedback of the regenerative braking energy. A large number of literatures have researched on the train operation optimization, including dynamic adjustment of the train running curve, the static optimization of the train diagrams [17], and an integration of both to achieve energy-efficient operations of multiple trains for metro lines [18]. In [19], the train diagram of Beijing Metro Line 5 is optimized taking the regenerative braking energy into account; however, the model of the traction power system only contains the ground-type braking resistors, the recovery of ESSs is not considered. Masafumi Miyatake *et al.* formulated the optimal operation problem of railway systems for minimum energy consumption considering system characteristics, and optimized the train speed profile as well as state of charge (SOC) profile of onboard ESS with dynamic programming (DP), gradient method and sequential quadratic programming (SQP) [20]. However, the influence of ESS sizing was not discussed. In [21], the train operation is optimized in the condition that the ESSs are installed in substations, but the charge and discharge energy of ESSs is estimated briefly without an accurate traction power system model, and the ESS capacity is also pre-determined. In [22], [23], the train diagram and ESS configuration are optimized collaboratively through GA. However, the optimization results under peak-hours and off-peak hours are obtained independently. In actual operation, the train headway varies with the passenger flow throughout the day. The braking energy distribution under different headways should be considered comprehensively during optimization. In addition, with ESSs installed in the urban rail system, a large amount of regenerative energy can be recovered in time by the ESSs, and the surge of the train's pantograph voltage will be effectively suppressed. Nevertheless, the early intervention of braking resistor obstructs the braking energy to be fed back to the traction network [24]–[26]. The above literatures don't consider the effect of traction power system parameters on regenerative braking energy recovery.

B. Main Contributions

Distinguished from previous works, this paper comprehensively considers the ESS capacity configuration, train operation and characteristics of substations and braking resistors, carries out theoretical analysis and collaborative optimizations from the systematic perspective. The main contributions of this work are summarized as follows:

1) The effects of traction power parameters on energy interactions between substations, ESSs and trains are revealed, and the multi-variable synthetic optimization is conducted to find the optimum system configurations based on the multi-train traction power simulator. In comparison with ESS-only optimization, it improves the regenerative energy utilization and system energy transmission efficiency, thus obtains better economic and energy-saving benefits.
2) A two-stage, multi-objective optimization framework is established, where the design variables and operation variables are optimized iteratively to tackle with the huge search space in direct optimization. In addition, the pareto frontier of the multi-optimization problem is obtained based on NSGA-II, presenting intuitionistic relationship and good trade-off between energy consumptions and ESS configuration cost, which can't be realized by single-objective optimizations.
3) Rather than in specific train operation scenario, this paper reveals the change regularities of energy consumptions under different headways, and presents optimization results in peak hours, off-peak hours and all-day considering the variation of traffic conditions throughout the day.

The remainder of this paper is organized as follows: First, the mathematical model of the urban rail traction power system with SCESSs is introduced, and the influences of system parameters on the energy consumption and regenerative braking energy distribution are analyzed quantitatively. Next, a two-layer multi-objective optimization model for system parameters is established, and the multi-parameter iterative optimization algorithm based on NSGA-II is presented. Finally, based on the parameters of Beijing Batong line, the optimization results with different algorithms are compared.

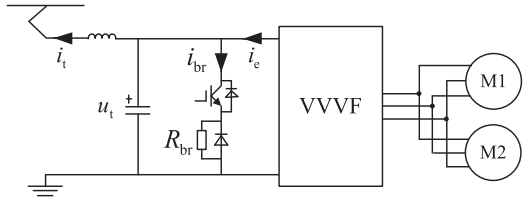

Fig. 1. The traction drive system of urban railway trains.

II. Mathematical Model of the System

A. The Urban Railway Trains

The traction drive system of trains is shown in Fig. 1. It's mainly composed of filter inductors and capacitors, traction converters, motors and on-board braking resistors. When the train is powering, it obtains electric energy from the traction network through the current collector; when the train is braking, the traction motors convert the mechanical energy into regenerative electric energy and feed it back to the network.

For the service braking of urban rail trains, the electro-pneumatic braking is generally used: the electrical braking is exerted in priority, and the pneumatic braking is added only when

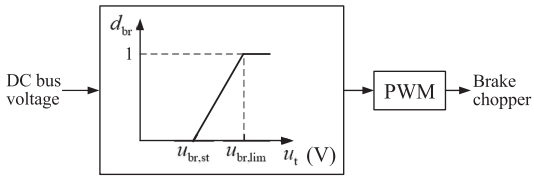

Fig. 2. The control scheme of onboard braking resistor.

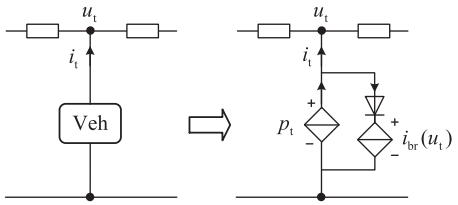

Fig. 3. The equivalent model of train.

the electrical braking is insufficient so as to meet the requirement of the total braking force command. The electric braking of the train is hybrid with regenerative braking and rheostatic braking: the regenerative braking energy is fed back to the traction power network (i.e., regenerative braking in priority) when the traction power of adjacent trains is larger than the train's braking power; otherwise when the traction power network is unable to absorb the regenerative braking energy, and the train voltage rises higher than the starting voltage of braking resistor, the braking resistor will be activated to consume the residual braking energy. The on-board braking resistor is composed of a braking chopper and a resistor. The train's controller controls the on and off of the brake chopper by detecting the DC bus voltage, and realizes the power distribution of regenerative braking and rheostatic braking [27]. The control scheme of braking resistor is shown in Fig. 2, where $d_{\rm br}$ is the duty cycle, $u_{\rm br,st}$ and $u_{\rm br,lim}$ are the starting voltage and limit voltage of the braking resistor respectively, $u_{\rm t}$ is the train DC bus voltage. It's seen from Fig. 2 that when $u_{\rm t}$ exceeds $u_{\rm br,st}$, the brake chopper starts, and $d_{\rm br}$ increases linearly with $u_{\rm t}$; when $u_{\rm t}$ rises to $u_{\rm br,lim}$, $d_{\rm br}$ reaches 1. And the average current of the braking resistor in a switch period is calculated by (1).

$$\bar{i}_{\rm br} = d_{\rm br} \cdot \frac{u_{\rm br}}{R_{\rm br}} \tag{1}$$

Therefore, considering the electrical characteristics of trains in the traction power system, the train is modeled as a controlled power source in parallel with a variable current source, as shown in Fig. 3. The relationship of the train collector current, voltage and power is formulated as (2).

$$i_{\rm t} = \frac{p_{\rm t}}{u_{\rm t}} - i_{\rm br}(u_{\rm t}) \tag{2}$$

Where $i_{\rm t}$ represents the train collector current, $p_{\rm t}$ represents the DC side power of the train's traction converter, and $i_{\rm br}$ denotes the current of braking resistor.

B. The SCESS

The SCESS consists of SC modules and a DC/DC converter. Considering the bi-directional energy flow and high-power applications, the bidirectional half-bridge converters are widely used [28], [29], as shown in Fig. 4. At two sides of the DC/DC converter, the voltage of SC modules is represented by $u_{\rm sc}$, and the voltage of traction network is denoted as $u_{\rm ess}$.

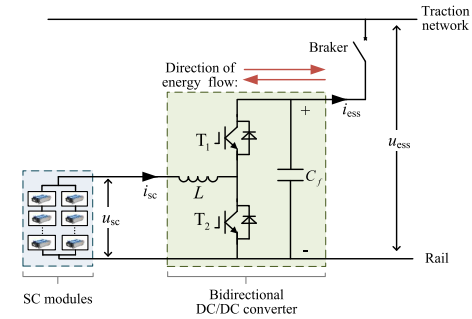

Fig. 4. The circuit structure of SCESS.

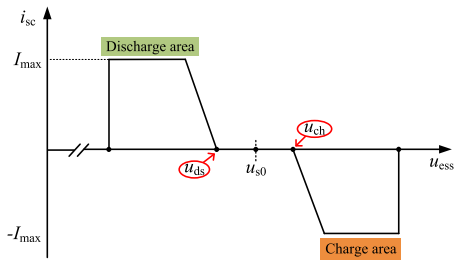

Fig. 5. The line-voltage-based control scheme of SCESS.

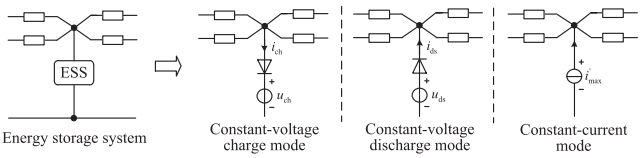

Fig. 6. The steady-state model of SCESS for traction network side.

In this paper, the line-voltage-based control scheme is adopted for SCESS, as seen in Fig. 5. $u_{\rm ch}$ is the charge voltage threshold, $u_{\rm ds}$ is the discharge voltage threshold of SCESS. When $u_{\rm ess} \geq u_{\rm ch}$, SCESS works in charge state to recover the regenerative energy; when $u_{\rm ess} \leq u_{\rm ds}$, SCESS works in discharge state, and provides energy for powering trains.

Considering the current limitations of SCESS in practical operation, the SCESS can work in voltage stabilization mode and constant current mode, i.e. when the SC current doesn't reach the maximum value, the double closed loop converter control stabilizes $u_{\rm ess}$ at $u_{\rm ch}$ or $u_{\rm ds}$, the SCESS is equivalent to a controlled voltage source in steady-state for the traction network side; and when the SC current reaches the maximum allowable current, the current limiter works, SC is charged or discharged with the maximum current. Then the SCESS is equivalent to a controlled current source for the traction power system, as shown in Fig. 6.

For the low-voltage side of SCESS, the first-order RC model is established to emulate the dynamic performance of SC [30]. The relationship between SC output voltage and current is formulated as (3) and (4).

$$u_{\rm c}(t) = C_{\rm sc}^{-1} \cdot \int_0^t i_{\rm sc}(\tau) d\tau + u_{\rm c0} \tag{3}$$

$$u_{\rm sc}(t) = u_{\rm c}(t) + r_{\rm sc} \cdot i_{\rm sc}(t) \tag{4}$$

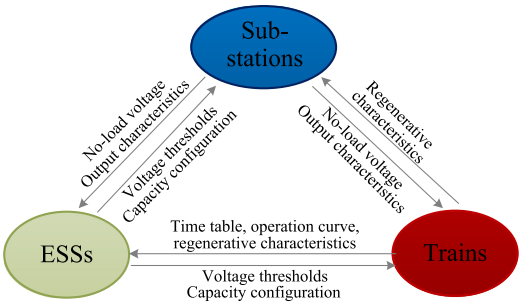

Fig. 7. The interaction between ESSs, trains and substations.

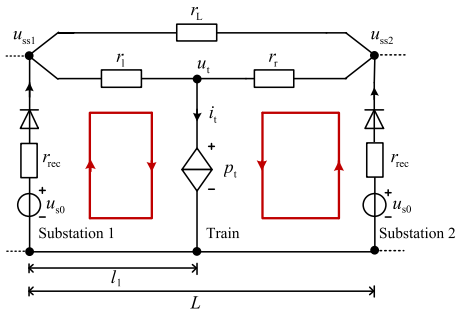

Fig. 8. The equivalent circuit model of single-train powering scenario.

Where C_{sc} and r_{sc} represent the SC capacitance and internal resistance, respectively; u_{sc} and i_{sc} are the SC terminal voltage and current. u_{c0} and $u_c(t)$ respectively denote the initial voltage and voltage at moment t of the capacitive part.

III. Influences of Traction Power Parameters on System Energy Transmission

In the traction power system with ESSs, energy of substations, ESSs and trains are transmitted to each other through the traction network, which is simultaneously affected by parameters of each part. Fig. 7 presents interaction relationship between them. The no-load voltage of substation determines the overall voltage level of the power supply system, and the starting voltage of the braking resistor affects the voltage rise of the power supply network and the consumption of regenerative energy on the braking resistors. Therefore, this section establishes equivalent circuit models for different train operating scenarios, and analyzes the influences of no-load voltage and braking resistor starting voltage on energy transmission between substations, powering/braking trains and ESSs.

A. Energy Transmission Between Substations and Powering Trains

Fig. 8 presents the equivalent model of the train operation scenario when single-train powering. The node voltage equation and voltage-current relationships of the system are formulated as (5) and (6), respectively.

$$\begin{cases} (u_t - u_{ss1}) \cdot r_l^{-1} + (u_t - u_{ss2}) \cdot r_r^{-1} + p_t/u_t = 0 \\ (u_{ss1} - u_t) \cdot r_l^{-1} + (u_{ss1} - u_{ss2}) \cdot r_L^{-1} \\ + (u_{ss1} - u_{s0}) \cdot r_{rec}^{-1} = 0 \\ (u_{ss2} - u_t) \cdot r_r^{-1} + (u_{ss2} - u_{ss1}) \cdot r_L^{-1} \\ + (u_{ss2} - u_{s0}) \cdot r_{rec}^{-1} = 0 \end{cases} \tag{5}$$

$$\begin{cases} i_{ss1} = (u_{s0} - u_{ss1}) \cdot {r_{rec}}^{-1} \\ i_{ss2} = (u_{s0} - u_{ss2}) \cdot {r_{rec}}^{-1} \end{cases} \tag{6}$$

Where:

$$\begin{cases} r_l = l_l \cdot r \\ r_r = (L - l_l) \cdot r \\ r = r_{contact} + r_{rail} \end{cases} \tag{7}$$

Where r denotes the unit line resistance, it's calculated by the sum of contact line unit resistance $r_{contact}$ and rail unit resistance r_{rail}, l_l and l_r represent the distances between the train and left/rignt substations, and L is the distance between two substations.

Solve the node voltage equations (5) to get the expressions of train collector voltage u_t, substation output voltages u_{ss1} and u_{ss2}, and substitute them into (6), then the output currents of two substations are obtained, as seen in (8) and (9).

$$i_{ss1} = \frac{\left(L \cdot r_{rec} \cdot (r_r + 2r_{rec})\,(r_L + 4r_{rec})\,u_{s0} - \sqrt{\Delta}\right)}{2r_{rec} \cdot (r_L + 2r_{rec})\,(r_L + 4r_{rec})\,(l_l \cdot r_r + L \cdot r_{rec})} \tag{8}$$

$$i_{ss2} = \frac{(r_l + 2r_{rec})\left(L \cdot r_{rec} \cdot u_{s0} \cdot (r_L + 4r_{rec})(r_r + 2r_{rec}) - \sqrt{\Delta}\right)}{2r_{rec} \cdot (r_L + 2r_{rec})\,(r_L + 4r_{rec})\,(r_r + 2r_{rec})\,(l_l \cdot r_r + L \cdot r_{rec})} \tag{9}$$

Where:

$$\Delta = L \cdot {r_{rec}}^2 (r_r + 2r_{rec})^2\,(r_L + 4r_{rec}) \cdot \left(L \cdot (r_L + 4r_{rec}) \cdot {u_{s0}}^2 - 4p_t\,(r_L + 2r_{rec})\,(l_r \cdot r_l + L \cdot r_{rec})\right) \tag{10}$$

The energy transmission efficiency between substations and the powering train can be calculated by the ratio of the train's traction power to the total output power of substations, as shown in (11).

$$\eta\,(u_{s0}) = \frac{p_t}{p_{ss1} + p_{ss2}} \tag{11}$$

Where p_t is the train's traction power, p_{ss1} and p_{ss2} are output powers of substation 1 and 2, respectively, as expressed in (12).

$$\begin{aligned} p_{ss1} &= u_{s0} \cdot i_{ss1} \\ p_{ss2} &= u_{s0} \cdot i_{ss2} \end{aligned} \tag{12}$$

Fig. 9(a) presents the surface of η when the train's traction power is 1MW. Fig. 9(b) shows the relationship of η and u_{s0} when the train is in the middle of the two substations, i.e., $l_l = l_r$. The system parameters are listed in Table I. It's seen from Fig. 9 that η rises with the increase of u_{s0}, and the efficiency improvement is more significant when the train's traction power is large: when $p_t = 1\,\mathrm{MW}$, and u_{s0} increases from 800 V to

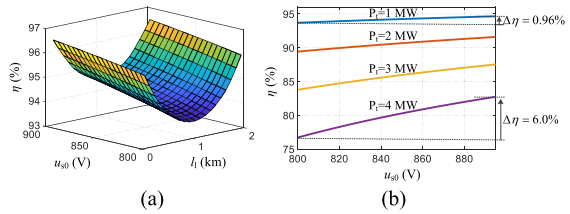

(a) (b)

Fig. 9. The transmission efficiency between substation and powering train.

TABLE I
PARAMETERS OF THE TRACTION POWER SYSTEM

Parameters	Values	Units
L	2	km
r_{contact}	0.0191	Ω/km
r_{rail}	0.017	Ω/km

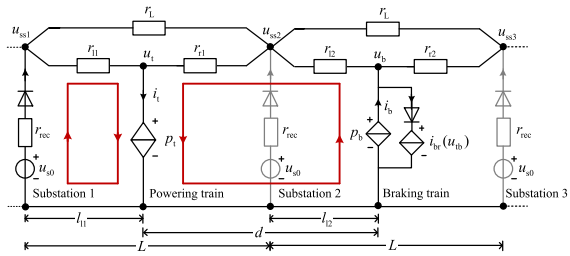

Fig. 10. The equivalent circuit model of the operation scenario with one powering train and one braking train.

900 V, η gets improved by 0.96%; when $p_{\text{t}} = 4\,\text{MW}$, η is increased by 6.0%.

B. Energy Transmission Between Powering and Braking Trains

For the train operation scenario when one train powering and one train braking, the equivalent circuit model of the system is shown in Fig. 10.

It's deduced from Fig. 10 that the circuit equation when the substation 2 is in standby state is expressed by (13), and it's formulated as (14) when the substation 2 is in operation state. The current of braking resistor i_{br} is calculated by (1).

$$\begin{cases} (u_{\text{ss1}} - u_{\text{t}}) \cdot {r_{\text{l1}}}^{-1} + (u_{\text{ss1}} - u_{\text{ss2}}) \cdot {r_{\text{L}}}^{-1} \\ + (u_{\text{ss1}} - u_{\text{s0}}) \cdot {r_{\text{rec}}}^{-1} = 0 \\ (u_{\text{t}} - u_{\text{ss1}}) \cdot {r_{\text{l1}}}^{-1} + (u_{\text{t}} - u_{\text{ss2}}) \cdot {r_{\text{r1}}}^{-1} + p_{\text{t}}/u_{\text{t}} = 0 \\ (u_{\text{ss2}} - u_{\text{t}}) \cdot {r_{\text{r1}}}^{-1} + (u_{\text{ss2}} - u_{\text{ss1}}) \cdot {r_{\text{L}}}^{-1} \\ + (u_{\text{ss2}} - u_{\text{b}}) \cdot {r_{\text{p2}}}^{-1} = 0 \\ (u_{\text{b}} - u_{\text{ss2}}) \cdot {r_{\text{p2}}}^{-1} = p_{\text{b}}/u_{\text{b}} - i_{\text{br}}\,(u_{\text{br,st}}, u_{\text{b}}) \end{cases} \tag{13}$$

$$\begin{cases} (u_{\text{ss1}} - u_{\text{t}}) \cdot {r_{\text{l1}}}^{-1} + (u_{\text{ss1}} - u_{\text{ss2}}) \cdot {r_{\text{L}}}^{-1} \\ + (u_{\text{ss1}} - u_{\text{s0}}) \cdot {r_{\text{rec}}}^{-1} = 0 \\ (u_{\text{t}} - u_{\text{ss1}}) \cdot {r_{\text{l1}}}^{-1} + (u_{\text{t}} - u_{\text{ss2}}) \cdot {r_{\text{r1}}}^{-1} + p_{\text{t}}/u_{\text{t}} = 0 \\ (u_{\text{ss2}} - u_{\text{t}}) \cdot {r_{\text{r1}}}^{-1} + (u_{\text{ss2}} - u_{\text{ss1}}) \cdot {r_{\text{L}}}^{-1} \\ + (u_{\text{ss2}} - u_{\text{s0}}) \cdot {r_{\text{rec}}}^{-1} + (u_{\text{ss2}} - u_{\text{b}}) \cdot {r_{\text{p2}}}^{-1} = 0 \\ (u_{\text{b}} - u_{\text{ss2}}) \cdot {r_{\text{p2}}}^{-1} = p_{\text{b}}/u_{\text{b}} - i_{\text{br}}\,(u_{\text{br,st}}, u_{\text{b}}) \end{cases} \tag{14}$$

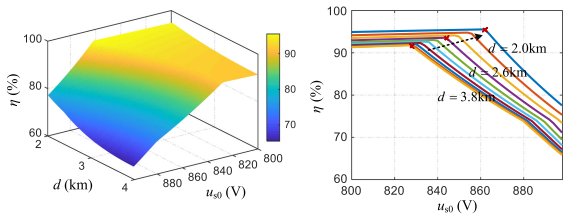

(a) (b)

Fig. 11. The relationship of substation no-load voltage and energy transmission effeciency between powering/braking trains.

Where:

$$\begin{cases} r_{\text{l1}} = r \cdot l_1 \\ r_{\text{L}} = r \cdot L \\ r_{\text{r1}} = r \cdot (L - l_1) \\ r_{\text{p2}} = r_{\text{l2}} \parallel (r_{\text{L}} + r_{\text{r2}}) \end{cases} \tag{15}$$

The power conservation equation of the system is deduced from Fig. 10, as seen in (16). The substations and braking train provide energy for the powering train simultaneously. In the energy transmission process, energy loss consists of line transmission loss and the energy dissipated on braking resistor. Thus the energy transmission efficiency between the powering train and braking train is formulated as (17).

$$p_{\text{ss1}} + p_{\text{ss2}} + p_{\text{b}} = p_{\text{t}} + p_{\text{line}} + p_{\text{br}} \tag{16}$$

Where p_{t} and p_{b} respectively represent the power of powering and braking trains, p_{line} is the line power loss, and p_{br} is the power of braking resistor.

$$\eta\,(u_{\text{s0}}, u_{\text{br,st}}) = \frac{p_{\text{t}}}{p_{\text{ss1}} + p_{\text{ss2}} + p_{\text{b}}} \tag{17}$$

First, the relationship of η and u_{s0} is analyzed. When p_{t} and p_{b} are both 1MW, and $u_{\text{br,st}} = 900\text{V}$, the surface of η is depicted in Fig. 11(a). It's noticed that there is a high-efficiency area where η is higher than 90%, outside which η reduces significantly and can be lower than 70%. Fig. 11(b) is the projection of η surface on the $x - z$ plane, it reveals the relationship of η and u_{s0} at different train distances. It's seen from Fig. 11(b) that there is a inflection point on the curve of η: before the inflection point, the line loss reduces with the increase of u_{s0}, so η increases monotonically; afterwards, the train collector voltage exeeds $u_{\text{br,st}}$ with the rise of system voltage, the braking resistor is activated and consumes the regenerative braking energy, as a result of which η reduces rapidly. Besides, when the distance between powering and braking trains is shorter, the voltage difference between two trains is smaller, and u_{s0} at the inflection point will be higher.

Fig. 12(a) shows the surface of η with $u_{\text{br,st}}$ and distance between two trains, and Fig. 12(b) is the projection in the y-z plane when $u_{\text{s0}} = 860\,\text{V}$. It's seen that at different train positions and no-load voltages, η rises with the increase of $u_{\text{br,st}}$. However, when the distance of two trains is long, there is also an inflection point on the curve of η. Take $d = 2.6\,\text{km}$ for example, when $u_{\text{br,st}}$ increases from 900 V to 916 V, η rises from 86.3% to 93.7%, which is improved by 7.4%; but afterwards η is hardly changed. This is because when $u_{\text{br,st}}$ exceeds 916 V, the collector voltage

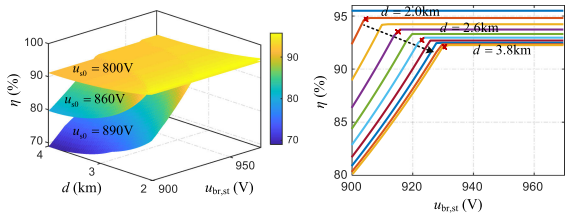

(a) (b)

Fig. 12. The relationship of transmission effeciency between powering/braking trains and start voltage of braking resistor.

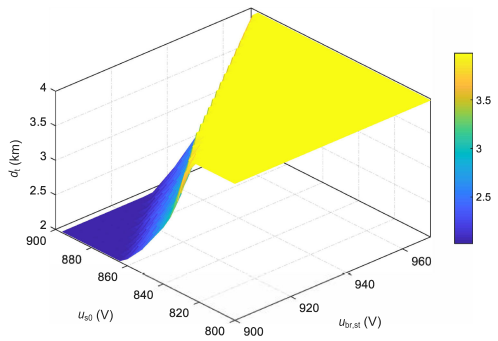

Fig. 13. The relationship of energy transmission distance between trains and parameters of substations and braking resistors.

of braking train doesn't reach $u_{\mathrm{br,st}}$, the braking resistor does not work, and the line transmission loss is not directly affected by $u_{\mathrm{br,st}}$. It's also observed from Fig. 12(b) that the efficiency inflection point moves right with the increase of d, illustrating that in order to improve the transmission efficiency between trains, the farther train distance is, the higher $u_{\mathrm{br,st}}$ should be.

It can be seen from Fig. 11 and 12 that there is a dividing line that is related to the distance between trains, which divides the energy efficiency surface into high-efficiency area and efficiency-decline area. In order to quantitatively analyze the influence of train distance on energy transmission efficiency, in this paper, the effective energy transmission distance between powering and braking trains is defined as the maximum train distance when the braking resistor does not start, and the regenerative energy is effectively utilized by powering train, as denoted by d_{t}. Substituting $u_{\mathrm{b}} = u_{\mathrm{br,st}}$ into (13) and (14), the relationship of d_{t}, u_{s0} and $u_{\mathrm{br,st}}$ is deduced, as seen in Fig. 13. It's observed from Fig. 13 that when u_{s0} and $u_{\mathrm{br,st}}$ are near 900 V, d_{t} is short, which is within 2 km; with the increase of difference between $u_{\mathrm{br,st}}$ and u_{s0}, d_{t} gets lengthened obviously; and when $u_{\mathrm{br,st}} - u_{\mathrm{s0}} > 72\,\mathrm{V}$, d_{t} exceeds 4 km, implementing efficient regenerative energy transmission between the powering and braking trains.

Through the circuit modeling and analysis of energy transmission, the following conclusions can be drawn:

1) The increase of no-load voltage reduces the transmission loss of power network, but it also leads to higher intervention frequency of braking resistors, and the effective regenerative energy transmission distance between trains gets shorter.

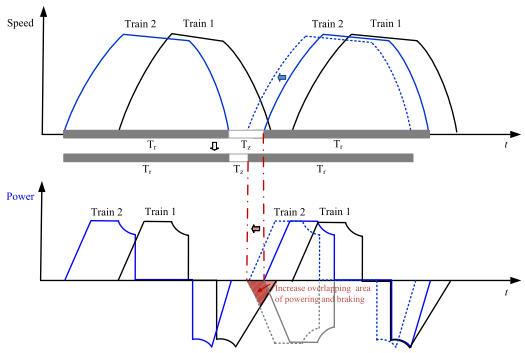

Fig. 14. The schematic diagram of dwell time adjustment to increase energy interaction between trains.

2) The intervention of braking resistor is delayed by increasing its start voltage, thus the regenerative energy transmission efficiency is improved, and the effective transmission distance gets longer within a certain range of $u_{\mathrm{br,st}}$. Therefore, optimizing $u_{\mathrm{br,st}}$ and u_{s0} collaboratively will realize effective utilization of regenerative energy, and further reduction of line transmission loss in the meanwhile.

IV. Influence of Train Operation Parameters on System Energy Distribution

In the traction power network with multiple trains in operation, the train's regenerative braking energy can be absorbed by ESSs installed in substations on the one hand, and utilized by adjacent powering trains on the other hand. The train operation diagram stipulates the arrival and departure times of trains at each station, thus determines the time and space distribution of trains, which has an important impact on the energy interaction and consumption of the system. In the design of train diagrams, if the dwell times are adjusted to incease the overlap of powering and braking trains on the premise of satisfying service and tracking interval restrictions, as seen in Fig. 14, more regenerative energy will be utilized by the adjacent powering trains, which effectively avoids waste of regenerative energy, and decreases the load requirements of ESSs, as a result of which the configuration power and capacity of ESSs can be significantly reduced.

In this paper, the influence of train operation parameters on the energy consumptions of the system is analyzed based on Batong Line, as seen in Fig. 20 in Section VI. The simulation process is implemented on the traction power system simulator with multi-train operation. The simulator is developed in Matlab/Simulink environment, it is capable of calculating the power flow of the traction power network with SCESSs in multi-train operation, and obtains the distribution of regenerative braking energy in the whole metro line. The flowchart of the simulator is depicted in Fig. 15, including the single-train traction calculation, multi-train operation simulation and DC power flow calculation. And the power conservation equation of the traction power system for the whole metro line can be expressed as (18).

$$\sum p_{\mathrm{ss,i}} + \sum p_{\mathrm{b,j}} + \sum p_{\mathrm{ds,k}}$$

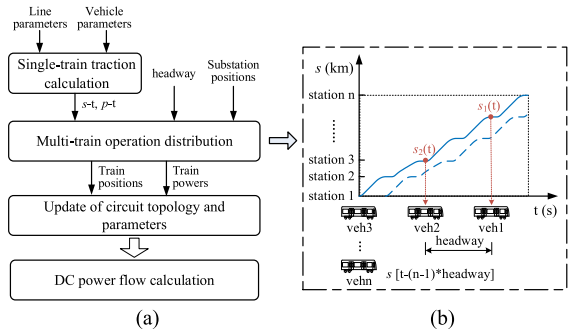

Fig. 15. The flowchart of the multi-train traction power simulator.

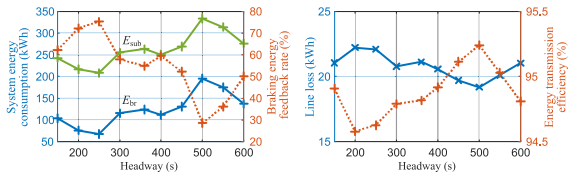

Fig. 16. The influence of train headway on energy consumptions.

$$= \sum p_{\mathrm{t,n}} + \sum p_{\mathrm{ch,m}} + p_{\mathrm{line}} + \sum p_{\mathrm{br,s}} \tag{18}$$

Where $p_{\mathrm{ds,k}}$ denotes the power of the k-th ESS in discharging state, and $p_{\mathrm{ch,m}}$ is the power of the m-th ESS in charging state.

A. Influence of Headway

Fig. 16 shows the curves of energy consumptions when the headway (denoted by H) increases from 150 s to 600 s. E_{sub} and E_{br} respectively denote the total output energy of substations along the whole metro line and the energy consumption on braking resistors. The braking energy feed-back rate R_{b} and energy transmission efficiency η are calculated by (19) and (20), respectively [31]. It's observed from Fig. 16 that with the increase of H, E_{sub} and E_{br} tend to increase as well, and R_{b} decreases; when $H = 250\,\mathrm{s}$, E_{sub} is 208.1 kWh, and when $H = 500\,\mathrm{s}$, E_{sub} increases to 333.3 kWh. This is because with the increase of H, the distance between trains is longer, so energy interaction between powering and braking trains reduces, more regenerative energy is dissipated on braking resistors, and more of the traction energy of powering trains is supplied by the traction substations. Besides, as other train operation parameters, such as dwell time, phase difference of upline and downline trains affect the distribution of regenerative energy as well, in intervals where H is smaller than 250 s and larger than 500 s, E_{sub} and E_{br} decrease a little with the increase of H. And it's observed from Fig. 16(b) that the line loss changes little with the variation of H, which keeps nearly 21 kWh, and the overall variation trend of line loss is in reverse with that of R_{b}, i.e. when more regenerative energy is fed back to the traction network, the line loss increases accordingly.

$$R_{\mathrm{b}} = \left(1 - \frac{E_{\mathrm{br}}}{E_{\mathrm{reg}}}\right) \times 100\% \tag{19}$$

$$\eta = \frac{E_{\mathrm{tra}}}{E_{\mathrm{sub}} + (E_{\mathrm{reg}} - E_{\mathrm{br}}) - \Delta E_{\mathrm{sc}}} \times 100\% \tag{20}$$

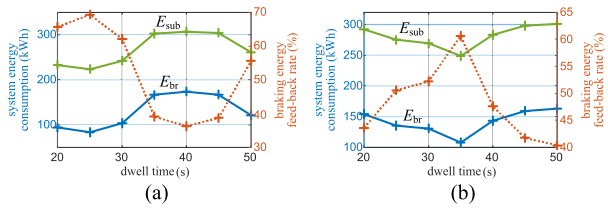

Fig. 17. The influence of train dwell time on energy consumptions under 180 s and 450 s headway.

Where E_{tra} and E_{reg} respectively represent the traction and regenerative energy of trains, and ΔE_{sc} is the change of stored energy in SC.

B. Influence of Dwell Time

Fig. 17(a) and (b) respectively display the relationship of system energy consumptions and train dwell time when the headway is 180 s and 450 s. It's seen that the dwell time has significant influence on energy consumptions, and it presents different regularity at different headways. When $H = 180\,\mathrm{s}$, E_{sub} and E_{br} increases with the increase of dwell time at first, when the dwell time exceeds 35 s, E_{sub} and E_{br} remain nearly unchanged, and after the dwell time is more than 45 s, E_{sub} and E_{br} decline gradually. Specifically, E_{sub} and E_{br} take the minimum values at 223.8 kWh and 83.8 kWh respectively when dwell time is 25 s, and R_{b} reaches 69.3%. However, when $H = 450\,\mathrm{s}$, E_{sub} and E_{br} decline first and increase afterwards with the increase of dwell time, the minimum energy point occurs at 35 s, where E_{sub} and E_{br} are 248.6 kWh and 107.9 kWh, respectively, and R_{b} is 60.6%.

C. Comprehensive Analysis of Train Operation and ESSs

Fig. 18(a) and (b) display the change of system energy consumptions with ESS configuration power at each station. The system overall energy consumption, E_{tot} is calculated by the difference of total output energy of substations and the change of stored energy of ESSs, as seen in (23). When $H = 180\,\mathrm{s}$, energy effectively interacts between trains due to high train density, the overall system energy consumption and energy consumption on braking resistors are 242.6 kWh and 103.6 kWh respectively without ESSs, and R_{b} is 62.1%. With the increase of ESS configuration power, the energy consumptions reduces gradually, and when the configuration power at each station increases to 5.2 MW, the energy consumptions keep almost unchanged. In comparison with that without ESSs, E_{tot} is 141.3 kWh, which is reduced by 101.3 kWh, and E_{br} decreases to 0.36 kWh, R_{b} reaches 99.87%. However, when $H = 450\,\mathrm{s}$, as less energy interacts between trains during off-peak hours, E_{tot} and E_{br} without ESSs are 269 kWh and 130.9 kWh respectively, which are larger than those during peak hours, and R_{b} is merely 52.2%. With the increase of ESS configuration power, the energy consumptions reduce rapidly, and keep almost constant when ESS configuration power is 1.57 MW. In comparison with those without ESS, E_{tot} is reduced by 127.1 kWh, and E_{br} is reduced to 0.01 kWh, illustrating that the braking resistors hardly start.

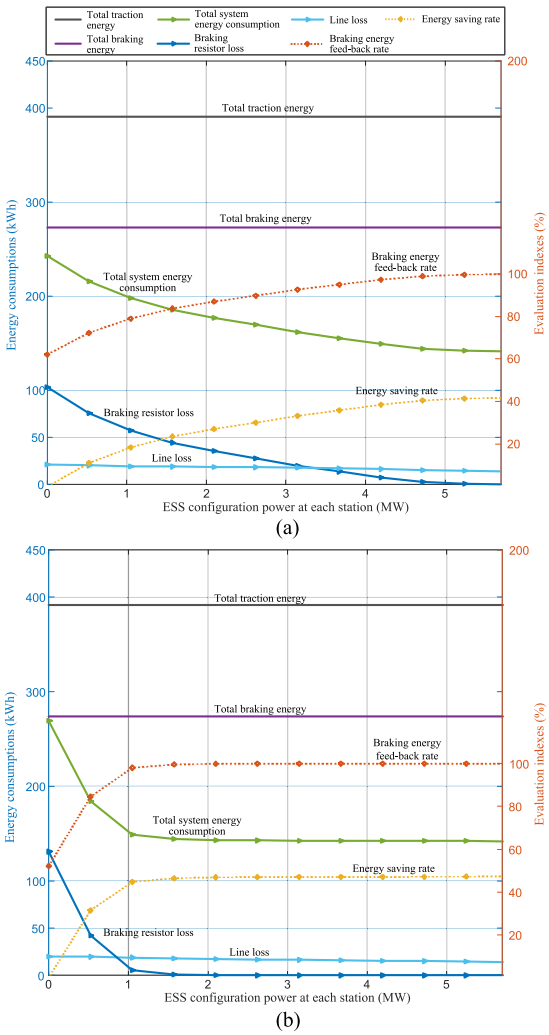

Fig. 18. The relationship between energy consumptions and configuration power of ESSs.

V. Synthetic Optimization for the System

It's seen from the above analysis that both the parameters of the traction power system and train operation have significant impacts on the transmission and utilization of regenerative braking energy, thus influence the capacity configuration requirements of ESSs. In addition, the system energy distributions under different train headways present different change regularity with train dwell time, ESS configuration power, etc. Therefore, a synthetic optimization method for ESS capacity, traction power system parameters and train operation is proposed in this paper considering the distribution characteristics of train headways throughout the day.

A. Synthetic Optimization Model

In the system synthetic optimization, the size of search space increases rapidly with the number of optimization variables, so direct optimization may become inefficient and difficult to converge to the optimal solution. Therefore, this paper proposes a two-layer optimization model. The upper layer is design parameter optimization, it aims to reduce the investment cost and improve the energy saving effect of ESSs by optimizing ESS capacity and traction power parameters. The optimization variable x is expressed by (21). It includes the parallel number of SC modules at each substation (denoted as $p_{\mathrm{sc,i}}$), u_{s0} and $u_{\mathrm{br,st}}$.

$$x = [p_{\mathrm{sc},1}, p_{\mathrm{sc},2}, \ldots, p_{\mathrm{sc,N}}, u_{\mathrm{s0}}, u_{\mathrm{br,st}}] \tag{21}$$

The objective function in the upper layer consists of two components, which is formulated as (22).

$$F = [E_{\mathrm{tot}}, COST_{\mathrm{ess}}] \tag{22}$$

The first component of F, i.e. E_{tot} is the total energy consumption of the system, which is calculated by (23). It reflects the energy saving effect of SCESSs, and is also positively correlated with the electricity cost of the traction power system from an economic point of view.

$$E_{\mathrm{tot}} = \sum_{i=1}^{N} \int_0^t i_{\mathrm{ss},i}(t) \cdot u_{\mathrm{ss},i}(t) dt - \frac{1}{2} \cdot \sum_{i=1}^{N} C_{\mathrm{sc},i} \cdot \left(u_{\mathrm{sc},i}^2(t) - u_{\mathrm{sc},i}^2(0)\right) \tag{23}$$

Where $i_{\mathrm{ss},i}(t)$ and $u_{\mathrm{ss},i}(t)$ are the current and voltage of the i-th substation at time state t. $C_{\mathrm{sc},i}$ is the total capacitance of supercapacitor, which is calculated by (24). $u_{\mathrm{sc},i}(t)$ is SC series voltage at time state t, and $u_{\mathrm{sc},i}(0)$ is SC series voltage at initial state. N is the number of substations.

$$C_{\mathrm{sc,i}} = p_{\mathrm{sc,i}} \cdot C_{\mathrm{rate}} / s_{\mathrm{sc,i}} \tag{24}$$

Where $p_{\mathrm{sc},i}$ is the i-th component of the optimization variable x. $s_{\mathrm{sc},i}$ is the series number, and C_{rate} is the rated capacitance of SC modules.

$i_{\mathrm{ss},i}(t)$, $u_{\mathrm{ss},i}(t)$ and $u_{\mathrm{sc},i}(t)$ in (23) can be obtained by solving the system equivalent circuit equations, as seen in (1)–(4) and (30). Considering the nonlinearty and time-varying characteristics of the system, it's hard to deduce the voltages and currents analytically. Therefore, in this paper, they are obtained from the multi-train traction power simulator numerically, as seen in Fig. 15. The basic parameters, including line parameters, vehicle parameters, etc., as well as the optimization variables are initialized, the simulator calculates the power flow of the system and obtain the voltages and currents at different nodes.

The second objective $COST_{\mathrm{ess}}$ is the total configuration cost of ESSs, which is the sum of the DC/DC converter cost and SC module cost at each substation, as shown in (25).

$$COST_{\mathrm{ess}}(x) = \sum_{i=1}^{N} \left(cost_{\mathrm{sc},i} + cost_{\mathrm{dcdc},i}\right) \tag{25}$$

Where $cost_{\mathrm{sc,i}}$ and $cost_{\mathrm{dcdc,i}}$ are the cost of SC module and DC/DC converter for the i-th substation, and they are calculated by (26) and (27), respectively.

$$cost_{\mathrm{sc,i}} = price_{\mathrm{sc}} \cdot s_{\mathrm{sc,i}} \cdot p_{\mathrm{sc,i}} \tag{26}$$

$$cost_{\mathrm{dcdc,i}} = price_{\mathrm{dcdc}} \cdot ceil\left(\frac{p_{\mathrm{sc,i}} \cdot I_{\mathrm{sc,rate}}}{I_{\mathrm{dcdc,rate}}}\right) \tag{27}$$

TABLE II
PARAMETERS OF THE CONSTRAINTS

Parameters	Values	Parameters	Values
$u_{\mathrm{br,min}}$	900 V	$soc_{\min}$	0.25
$u_{\mathrm{br,max}}$	1000 V	$soc_{\max}$	0.9
$u_{\mathrm{s0,min}}$	800 V	$t_{\mathrm{z,min}}$	20 s
$u_{\mathrm{s0,max}}$	900 V	$t_{\mathrm{z,max}}$	45 s

Where $price_{\mathrm{sc}}$ is the price of SC module, $price_{\mathrm{dcdc}}$ is the price of DC/DC module, $I_{\mathrm{sc,rate}}$ and $I_{\mathrm{dcdc,rate}}$ are the rated currents of SC module and DC/DC module, respectively.

The lower layer is operation optimization, where the system energy consumption is further reduced by optimizing the operation of trains and ESSs. It's deduced from Section II-B that the voltage thresholds of ESSs, i.e. u_{ch} and u_{ds} affect the power distribution between substations, trains and SCESSs, and are critical to the optimization of regenerative energy recovery. Therefore, the optimization variable in lower layer y consists of the train dwell time at each passenger station and voltage thresholds of ESSs, as depicted in (28). And the objective function of lower layer is also calculated by (23).

$$y = [t_{\mathrm{z1}}, t_{\mathrm{z2}}, \ldots, t_{zM}, u_{\mathrm{ch}}, u_{\mathrm{ds}}] \tag{28}$$

Where t_{zi} denotes the dwell time at the i-th station, M is the number of passenger stations along the metro line.

Therefore, the two-layer synthetic optimization model is formulated as (29). The constraints contain two parts: the equivalent circuit equations and the operation restrictions of the system. The former includes the system dynamic equations, as seen in (1)–(4), and the modified nodal voltage equations of the traction power system for the whole metro line considering the constant voltage sources [32], as represented by (30). The latter includes restrictions of SC parallel number, current and SOC, permissible ranges of u_{s0}, $u_{\mathrm{br,st}}$, t_{zi}, u_{ch} and u_{ds}.

$$\begin{aligned}
\min_{x\in\Re^n}\min_{y\in\Re^n}\quad & F(x,y) = [E_{tot}(x,y), COST_{ess}(x)] \\
\text{s.t.}\quad & (1)-(4)\ \text{and}\ (30) \\
& u_{\mathrm{br,min}} \le u_{\mathrm{br,st}} \le u_{\mathrm{br,max}} \\
& u_{\mathrm{s0,min}} \le u_{\mathrm{s0}} \le u_{\mathrm{s0,max}} \\
& 0 \le p_{\mathrm{sc}(1,\cdots,\mathrm{N})} \le p_{\mathrm{sc,max}} \\
& soc_{\min} \le soc_{1,\cdots,\mathrm{N}} \le soc_{\max} \\
& \left|i_{\mathrm{sc}(1,\cdots,\mathrm{N})}\right| \le I_{\mathrm{sc,rate}} \cdot p_{\mathrm{sc}(1,\cdots,\mathrm{N})} \\
& t_{\mathrm{z,min}} \le t_{\mathrm{z}(1,\cdots,\mathrm{M})} \le t_{\mathrm{z,max}} \\
& u_{\mathrm{s0}} < u_{\mathrm{ch}} < u_{\mathrm{br,st}} \\
& 0 < u_{\mathrm{ds}} < u_{\mathrm{s0}}
\end{aligned} \tag{29}$$

Where $u_{\mathrm{br,min}}$, $soc_{\min}$, $u_{\mathrm{s0,min}}$ and $t_{\mathrm{z,min}}$ are lower limits of $u_{\mathrm{br,st}}$, soc, u_{s0} and t_{z}, respectively. And $u_{\mathrm{br,max}}$, $soc_{\max}$, $u_{\mathrm{s0,max}}$, $p_{\mathrm{sc,max}}$ and $t_{\mathrm{z,max}}$ are upper limits. The values of them are listed in Table II. And $p_{\mathrm{sc,max}}$ is set at 115 for the SC module in Table III considering the substation space limits.

$$\begin{cases} Y_{\mathrm{n}} \cdot \begin{bmatrix} U_{\mathrm{sn}} \\ U_{\mathrm{t}} \end{bmatrix} = \begin{bmatrix} U_{\mathrm{s0}}/r_{\mathrm{rec}} \cdot D + I_{\mathrm{ess}} \\ I_{\mathrm{t}} \end{bmatrix} \\ U_{\mathrm{sn,cv}} = U_{\mathrm{ref}} \end{cases} \tag{30}$$

Where Y_{n} is the node admittance matrix of the system. U_{sn} and U_{t} respectively represent the voltage vectors of substation nodes and train nodes. D is the state vector of traction substations. $D(i) = 1$ means the i-th substation is in working state, and $D(i) = 0$ represents standby state. I_{ess} is the current vector of ESS branches, and I_{t} denotes the current vector of train branches. $U_{\mathrm{sn,cv}}$ is the voltage vector of the substation nodes where the ESSs work in voltage stabilization mode. U_{ref} is the voltage reference vector, $u_{\mathrm{ref}}(k) = u_{\mathrm{ch}}$ if the k-th ESS of $U_{\mathrm{sn,cv}}$ is in charge state; and $u_{\mathrm{ref}}(k) = u_{\mathrm{ds}}$ if in discharge state.

TABLE III
PARAMETERS OF SUPERCAPACITOR ENERGY STORAGE SYSTEM

Parameters	Values	Units
SC module type	BMOD0083 P048	-
C_{rate}	165	F
$I_{\mathrm{sc,rate}}$	130	A
$U_{\mathrm{sc,rate}}$	48	V
$price_{\mathrm{sc}}$	3,500	yuan
$I_{\mathrm{dcdc,rate}}$	500	A
$price_{\mathrm{dcdc}}$	250,000	yuan

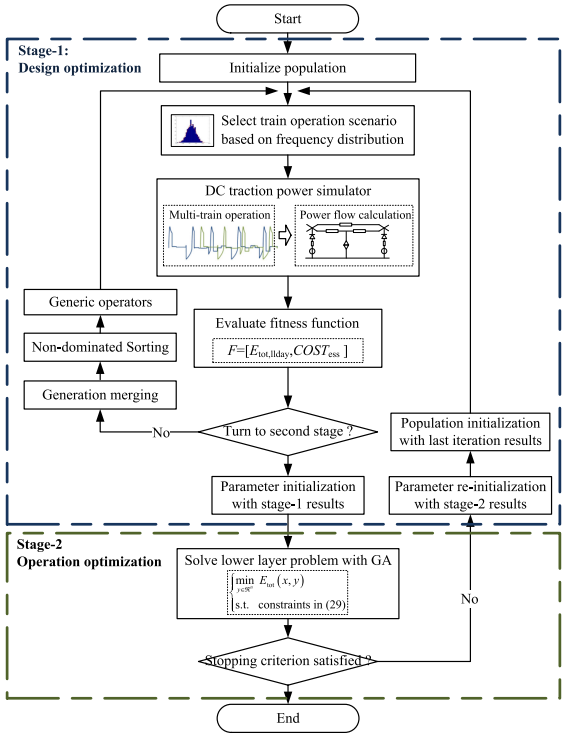

Fig. 19. The flowchart of proposed two-stage synthetic optimization algorithm.

B. Two-Stage Optimization Algorithm

This paper proposes a two-stage synthetic optimization algorithm (TS-OPT) to solve the two-layer optimization problem. The algorithm flowchart is presented in Fig. 19. In the first stage, considering the time-varying, nonlinear, discontinuity and multi-objective characteristics of the optimization model, the traditional analytical optimization algorithms, such as convex optimization are not applicable. Therefore, NSGA-II, which is one sort of multi-objective optimization algorithms based on GA, and has the advantages of high operation efficiency and

good convergence [33], is combined with the traction power simulator to search the pareto set. The random heuristic algorithm is effective to solve the complex engneering optimization problem. However, the global optimum cannot be guaranteed, and it's important to improve the goodness of the solution. The traction power simulator emulates the operation of the traction power system with SCESSs, obtains the system energy distribution, and then evaluates the optimization objective functions. In particular, the frequency distribution of the train headways throughout the day is deduced in this paper based on the train diagram, and the evaluation indexes of energy consumptions for the whole day are obtained by combining the occurrence frequency numbers and energy consumptions of different train operation scenarios, as shown in (31). In the operating process of NSGA-II, the population is stratified by fast non-dominated sorting; and the crowding degree of each individual in the non-dominated layer is calculated, the crowding-degree-comparison operator selects the individuals to form a new parent population, which helps maintain the population diversity, then the elite strategy is used in the algorithm to combine the parent and child populations to prevent missing of good individuals, the objective function is improved through the genetic operations including selection, crossover and mutation, and a new generation is generated. The pareto set of the multi-objective optimization problem is obtained after a number of iterations. The algorithm turns to the second stage. Based on the results of ESS capacity configuration and power supply parameters obtained in the first stage, the operation optimization problem in lower layer is solved by GA. If the algorithm stopping criterions are not satisfied, the design parameters of the first stage are re-optimized taking the optimization results of second stage as the initial conditions. Several iterations between the two stages are performed until the stopping criterions are satisfied, and then the synthetic optimization results for the system are obtained.

$$E_{\text{tot,allday}} = \sum_{k=1}^{S} E_k \cdot fn_k \tag{31}$$

Where $E_{\text{tot,allday}}$ is the system energy consumption in one day, E_k and fn_k respectively denote the energy consumption and frequency number of the k-th operation scenario, S is the number of typical train operation scenarios. E_k is calculated by initializing the input headway of the traction power simulator in Fig. 15 as the headway value H_k at the k-th operation scenario, and substituting the time period of the k-th operation scenario, i.e. $[0, H_k]$ into (23).

VI. Simulation Studies

A. Simulation Conditions

In this section, the proposed synthetic optimization algorithm is verified based on Batong Line. Fig. 20 shows the map pf Batong Line. It consists of 13 passenger stations, where 11 of them are traction substations. Fig. 21(a) and (b) respectively present the single-train operation curves upline and downline.

Fig. 22 presents the headway curve of Batong line. It's observed that peak hours arise during 6:50–9:00 and 16:50–17:20,

Fig. 20. The route map of Beijing Batong Line.

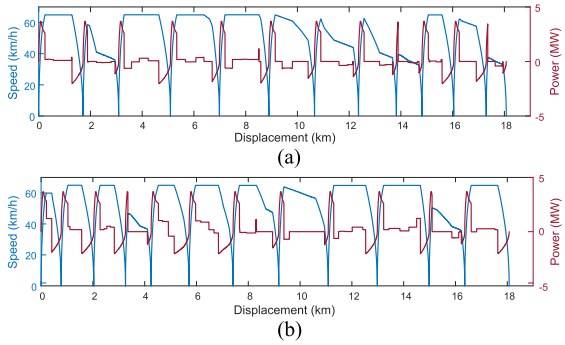

Fig. 21. The train operation curves along the whole metro line.

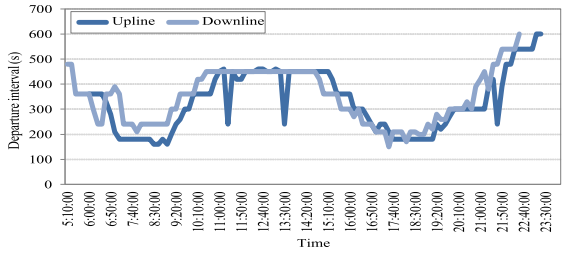

Fig. 22. The headway of Batong Line throughout the day.

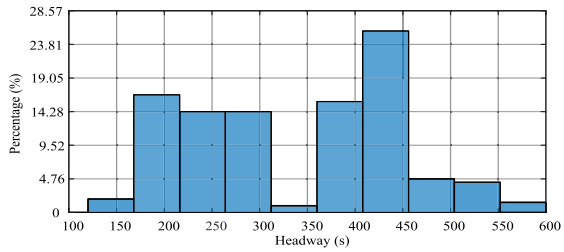

Fig. 23. The frequency distribution of headways of Batong Line.

where H is short, which is around 200 s; and during time intervals of 11:00–14:20 and later than 22:00 at night, the passenger flow density is low and H ranges from 450 s to 600 s. Fig. 23 shows the frequency distribution of the headway during one day. The traffic scenario when $H = 450$s has the highest frequency, which accounts for 26% of operation time in one day. In addition, the occurence frequency when H is less than 150 s or more than 500 s is relatively small.

Table III lists the parameters of SCESS. MAXWELL's BMOD0083 P048 module, with $I_{\text{sc,rate}}$=130 A and rated voltage $U_{\text{sc,rate}} = 48$ V is used for configuration, each costs 3,500 yuan. The price of DC/DC converter is 250,000 yuan per module with rated current of 500 A. The SC series number at each station, i.e., $s_{\text{sc,i}}$ is fixed at 14, and the ESS capacity is changed by modifying $p_{\text{sc,i}}$.

TABLE IV
COMPARISON OF TRAIN DWELL TIMES BEFORE AND AFTER OPTIMIZATION UNDER 180 S HEADWAY

Stations	t_z (Before optimization)		t_z (DS-OPT)		t_z (TS-OPT)	
	Upline (s)	Downline (s)	Upline (s)	Downline (s)	Upline (s)	Downline (s)
Sihui	30	30	30	30	30	30
Sihuidong	30	30	38	31	36	38
Gaobeidian	30	30	36	35	45	20
Chuanmeidaxue	30	30	35	34	38	43
Shuangqiao	30	30	35	30	31	38
Guanzhuang	30	30	27	33	36	24
Baliqiao	30	30	28	31	45	21
Tongzhoubeiyuan	30	30	34	35	37	38
Guoyuan	30	30	34	35	21	22
Jiukeshu	30	30	31	37	20	40
Liyuan	30	30	30	29	28	20
Linheli	30	30	32	31	29	38
Tuqiao	30	30	30	30	30	30
Total operation time (s)	1880	1818	1910	1849	1916	1830

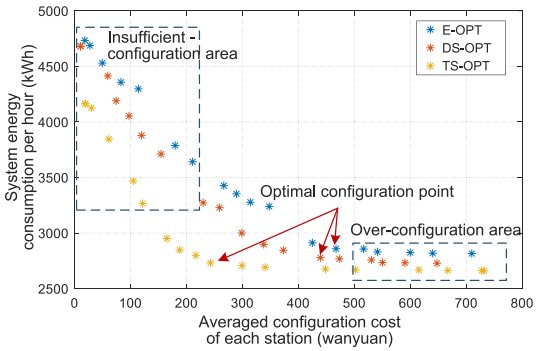

Fig. 24. The pareto curves of different multi-objective optimization methods under 180 s headway.

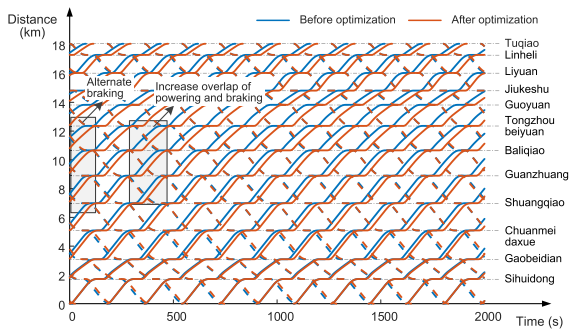

Fig. 25. Comparison of train diagrams under 180 s headway.

B. Simulation Results

As headway infuences system energy interaction, the capacity configuration requirements of ESSs will also differ. Therefore, in this paper, the optimization results of peak-hours ($H = 180$ s), off-peak hours ($H = 450$ s) and the whole day are compared and analyzed.

1) Peak Hours: Fig. 24 shows the pareto curves under ESS-only optimization (E-OPT), direct synthetic optimization (DS-OPT) and the two-stage synthetic optimization (TS-OPT) proposed in this paper when $H = 180$ s. It's observed that all of the pareto curves under the three optimization schemes have inflection points, which divide the pareto curves into insufficient-configuration area and over-configuration area. In the insufficient-configuration area, the ESSs are utilized effectively, and the system energy consumption per hour (denoted as $E_{\mathrm{tot,hour}}$) decreases rapidly with the increase of averaged ESS configuration cost at each station (denoted as C_{avg}). However, in the over-configuration area, $E_{\mathrm{tot,hour}}$ remains almost unchanged when C_{avg} continues to increase, which results in a waste of investment cost. Therefore, comprehensively considering the economic and energy-saving benefits, this paper takes the inflection point of the pareto curve as the optimum capacity configuration point. It's also obtained by comparing results of the three optimization schemes that synthetic optimizations effectively reduce system energy consumption compared with ESS-only optimization at the same ESS configuration cost. And ESS configuration costs under synthetic optimizations are lower than that of E-OPT with the same system energy consumption. In addition, TS-OPT proposed in this paper obtains a better pareto frontier compared to DS-OPT.

Table IV lists the train dwell times at each station before and after optimization, and Fig. 25 are the train diagrams. It's seen from Table IV that the train dwell times at each station after optimization satisfy the constraint range of 20–45 s, and the total operation times for the whole metro line are increased slightly, which are within 1 min. And comparing the train diagrams in Fig. 25, it's observed that before optimization, there are train operation scenarios when both upline and downline trains are braking simultaneously, the superposition of braking powers causes high recovery power requirement of ESSs. And after synthetic optimization, the arrival time of the upline train is delayed, so the trains arrive at station alternately, the ESS configuration requirement is significantly reduced. In addition, after adjustment of the train diagram, the overlapping time when the downline train in the section of Tongzhoubeiyuan-Shuangqiao is braking, and the upline train is powering is also prolonged, which effectively increases energy interaction between the braking and powering trains.

Fig. 26 shows the histograms of ESS configuration power at each station under three optimization methods. It's seen that after synthetic optimization of train diagram, traction power

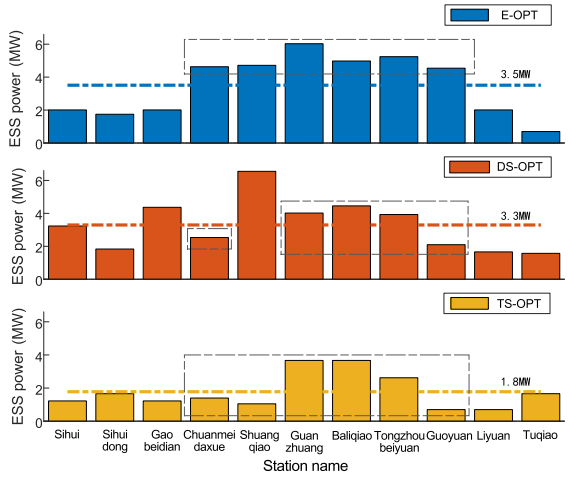

Fig. 26. The optimized capacity configurations of ESSs under 180 s headway.

TABLE V
COMPARISON OF POWER SYSTEM PARAMETERS BEFORE AND AFTER OPTIMIZATION UNDER 180 S HEADWAY

Parameters	Before optimization	DS-OPT	TS-OPT
u_{s0} (V)	860	852	843
$u_{br,st}$ (V)	900	935	920
u_{ch} (V)	865	871	865
u_{ds} (V)	855	839	815

TABLE VI
COMPARISON OF EVALUATION INDEXES UNDER 180 S HEADWAY

Methods	C_{avg} (wanyuan)	$E_{tot,hour}$ (kWh/h)
E-OPT	467	2859
DS-OPT	439	2778
TS-OPT	243	2731

parameters and ESS capacity, the spatial and temporal distribution of regenerative energy gets changed, so the ESS configuration results differ a lot from that of ESS-only optimization. Under E-OPT, the ESS powers at Chuanmeidaxue, Shuangqiao, Guanzhuang, Baliqiao, Tongzhoubeiyuan and Guoyuan stations all exceed 4 MW, and the averaged power at each station is 3.5 WM. However, under DS-OPT, the averaged power is reduced to 3.3 MW, and the ESS powers at Chuanmeidaxue and Guoyuan stations are reduced to 2.5 MW and 2.1 MW, respectively. Under TS-OPT, the ESS powers at the six stations from Chuanmeidaxue to Guoyuan are further decreased, and the averaged power is reduced to 1.8 MW.

Table V lists the substation no-load voltage and the starting voltage of braking resistor before and after optimization. It's seen from Table V that before optimization, $u_{br,st}$ is 40 V higher than u_{s0}. However, after DS-OPT and TS-OPT, the difference between $u_{br,st}$ and u_{s0} increases to 83 V and 77 V, respectively, so the intervention of braking resistor is delayed, and more of the regenerative energy is fed to the traction network, utilized by powering trains or recovered by ESSs.

Table VI compares the results of C_{avg} and $E_{tot,hour}$ under the three optimization schemes. It's observed that compared with E-OPT, both C_{avg} and $E_{tot,hour}$ are significantly reduced under synthetic optimizations. And C_{avg} under TS-OPT is further

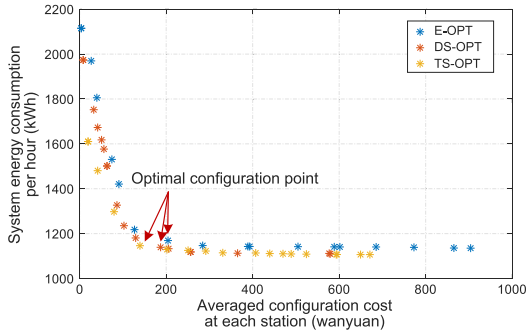

Fig. 27. The pareto curves under 450 s headway.

reduced by 196 wanyuan while $E_{tot,hour}$ under the two synthetic optimizations differ only by 47 kWh, which verifies that TS-OPT proposed in this paper reduces the search space for each stage by iterative process, thus improves the search efficiency of the optimization algorithm, and obtains better optimization results than direct optimization.

2) Off-Peak Hours: Fig. 27 compares the pareto frontiers when $H = 450$ s. Similar to previous analysis, the inflection points of the pareto curves are regarded as the optimum configuation points. It's seen from Fig. 27 that compared with the result of E-OPT, the synthetic optimizations obtain better pareto frontiers. In addition, by comparing the three pareto curves, it's observed that the optimization of power system parameters and train diagram has a significant effect on the reduction of system energy consumption when configuration power of ESS is small; and with the increase of ESS configuration power, more regenerative braking energy will be recovered by ESSs, thus the effect of power supply parameter and train diagram optimization is reduced. However, the synthetic optimization results remain better than that of ESS-only optimization. Besides, the inflection points of the pareto curves under synthetic optimizations move to the left, verifying that synthetic optimizations effectively reduce the ESS configuration cost on the premise that the system energy consumption is low. Also, by comparing Fig. 27 and Fig. 24, it's seen that in the insufficient-configuration area, the system energy consumption decreases more rapidly when $H = 450$ s: $E_{tot,hour}$ is reduced by 7.3 kWh when C_{avg} is increased by 10,000 yuan. However, when $H = 180$ s, the change rate of $E_{tot,hour}$ deceases to 5.0 kWh/10,000 yuan. This is because the train density is small when the headway is large, so less energy interacts between trains, and most of the regenerative energy will be absorbed by the ESSs after installation of ESSs, and the ESSs are utilized effectively. However, when the headway is small, there is complex energy interaction between trains, the energy-saving effect of ESSs is improved only when ESSs recover the part of regenerative energy that cannot be used by powering trains. In addition, with the increase of train density, the probability of train simultaneous powering and braking is higher, which enhances the ESS configuration requirements.

Fig. 28 presents the optimization results of ESS power configurations. Comparing with the results when $H = 180$ s, it's seen that the overall configuration power of ESSs is lower when $H = 450$ s. Under E-OPT, the averaged ESS power at each station is 1.45 MW, and Chuanmeidaxue Station has the largest ESS

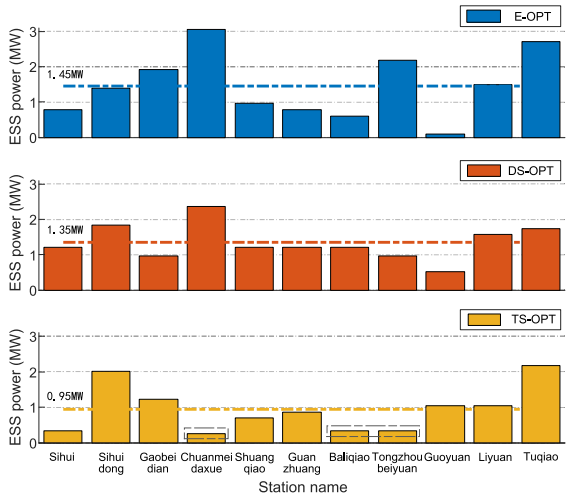

Fig. 28. The optimized capacity configurations of ESSs under 450 s headway.

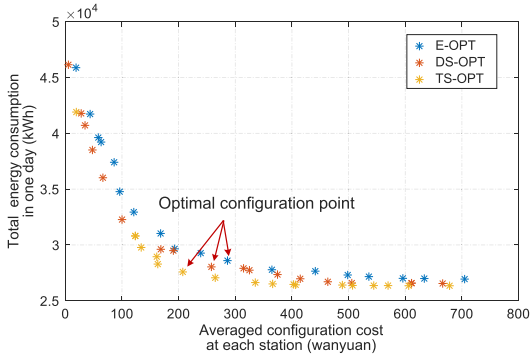

Fig. 29. The pareto curves for the whole day.

power of 3.06 MW. After DS-OPT and TS-OPT, the averaged ESS powers are reduced to 1.35 MW and 0.95 MW, respectively. As optimization of train diagram increases the overlapping time of powering and braking of trains in the two sections of Tongzhoubeiyuan-Baliqiao and Baliqiao-Guanzhuang, the ESS powers at Tongzhoubeiyuan and Baliqiao under TS-OPT are reduced by 1.84 MW and 0.26 MW respectively in comparison with E-OPT.

3) All-Day: It's seen from the optimization results of peak hours and off-peak hours that the optimized capacity of ESSs are not the same under different traffic conditions. Therefore, in this section, the capacity configuration of ESSs considering all-day operating is optimized based on the frequency distribution characteristics of the headways of Batong Line (as seen in Fig. 23 in Section V-B). Considering the large amount of calculation, four typical headways, including $H = 180$ s, 240 s, 450 s, and 550 s are selected to represent train operation scenarios of peak-hours and off-peak hours to reduce the computation time while well reflecting the all-day train operation characteristics. And the number of typical train operation scenarios S in (31) is 4 in this study. Fig. 29 shows the pareto curves under three optimization schemes for all-day. Similar to the analysis when the headway is 180 s and 450 s, the inflection points of the pareto curves are regarded as the optimum capacity configuration points. As the all-day optimization results comprehensively consider the regeneration energy recovery effects at different headways, its optimum point lies between the optimum points for peak-hours and off-peak hours; and compared with the other two optimization methods, the proposed two-stage synthetic optimization achieves the lowest configuration cost and system energy consumption.

TABLE VII
COMPARISON OF VOLTAGE PARAMETERS FOR ALL-DAY OPTIMIZATION

Methods	Voltage values (V)			
	u_{s0}	$u_{br,st}$	$u_{ch,allday}$	$u_{ds,allday}$
ES-OPT	860	900	[865,865,865,865]	[855,855,855,855]
DS-OPT	857	944	[865,868,869,868]	[851,845,839,851]
TS-OPT	830	934	[852,847,843,844]	[803,818,803,821]

TABLE VIII
ESS CAPACITY CONFIGURATION RESULTS UNDER DIFFERENT OPTIMIZATION SCHEMES FOR WHOLE DAY

Stations	Configuration powers (MW)		
	E-OPT	DS-OPT	TS-OPT
Sihui	4.0	0.1	1.0
Sihuidong	0.7	0.6	0.9
Gaobeidian	1.5	2.4	1.0
Chuanmeidaxue	2.6	3.7	0.4
Shuangqiao	3.1	2.8	2.4
Guanzhuang	2.4	3.9	0
Baliqiao	1.9	1.8	2.2
Tongzhoubeiyuan	1.5	0.7	3.1
Guoyuan	1.7	2.2	2.4
Liyuan	1.6	0.9	1.2
Tuqiao	2.2	1.6	2.0
Averaged value	2.1	1.9	1.5

Table VII compares the traction power parameters and ESS voltage thresholds for all-day optimization. Considering the differences in train operating characteristics, independent voltage thresholds are used for different headways. $u_{ch,allday}$ and $u_{ds,allday}$ represent the all-day charging and discharging voltage threshold sequences, including threshold values when the headway is 180 s, 240 s, 450 s and 550 s. It's seen from Table VII that the difference between u_{s0} and $u_{br,st}$ is increased after synthetic optimization, so the intervention of braking resistors is delayed. Under DS-OPT, the charging thresholds at different headways are closer to u_{s0}, and the differences are within 12 V. However, under the two-stage optimization, the charging threshold of ESSs in peak-hours is 22 V higher than u_{s0}, so energy interaction between trains is increased; and the charging threshold is lower in off-peak hours to recover the regenerative energy as much as possible. Therefore, the two-stage synthetic optimization improves the distribution of regenerative energy between ESSs and powering trains, has a better utilization of ESSs, and achieves more efficient braking energy recovery.

Table VIII lists the ESS capacity configurations at each station under the three optimization methods. Under E-OPT, the averaged configuration power at each station is 2.1MW (17.8kWh of energy). Compared with E-OPT, the configuration capacities of ESSs at Sihui, Tongzhoubeiyuan, Liyuan and Tuqiao stations are significantly reduced under DS-OPT, the averaged power at each station is reduced to 1.9 MW (15.9 kWh) and under

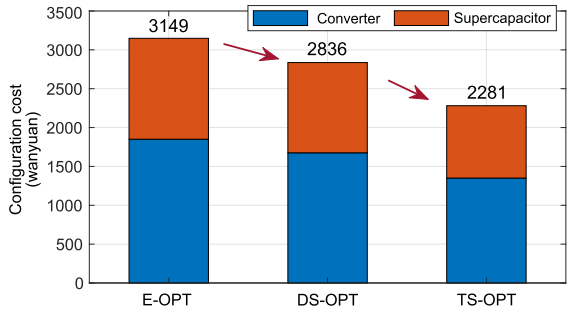

Fig. 30. Comparison of configuration costs under different optimization schemes for whole day.

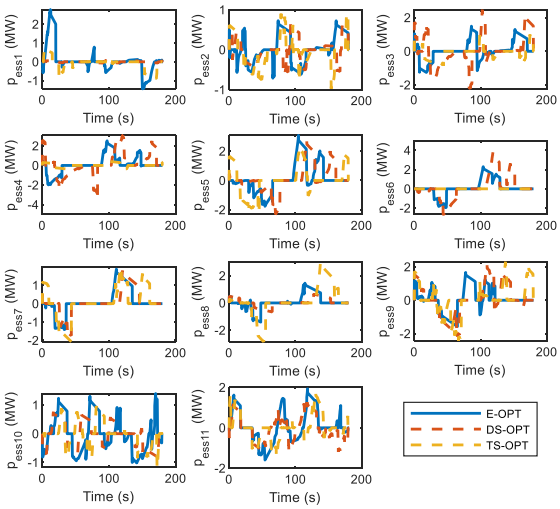

Fig. 31. The power curves of SCESSs along the metro line when $H = 180$ s.

TS-OPT, ESS configuration powers at Sihui, Sihuidong, Gaobeidian, and Chuanmeidaxue stations are within 1 MW, while no ESS is installed at Guanzhuang Station, and the averaged ESS power at each station is further reduced to 1.5MW (12.8kWh). Fig. 30 compares the ESS configuration costs under three optimization schemes. Under E-OPT, the total configuration cost for the whole line is 31.49 million yuan, in which the cost of DC/DC converter is 18.5 million yuan and the cost of SC module is 12.99 million yuan; however, the total cost after DS-OPT and TS-OPT are respectively reduced by 3.13 and 8.68 million yuan, verifying that multi-variable synthetic optimizations can effectively reduce the ESS investment under all-day operating condition.

Fig. 31 and 32 display the SC power and SOC curves at different substations along the whole metro line when $H = 180$ s, and Fig. 33 shows the total powers of trains, SCESSs, substations and braking resistors. It's seen from Fig. 31 and 32 that under E-OPT, the SCESSs tend to charge as soon as possible. Therefore, during 50-100 s, SCESSs at the 3rd -9th stations are fully-charged, a large amount of regenerative energy is dissipated on braking resistors, and the maximum total power of braking resistors reaches 6MW, as seen in Fig. 33(a). In addition, the capacity utilization of SCESS at the first substation (Sihui) is low. However, under DS-OPT and TS-OPT, the SCESSs are

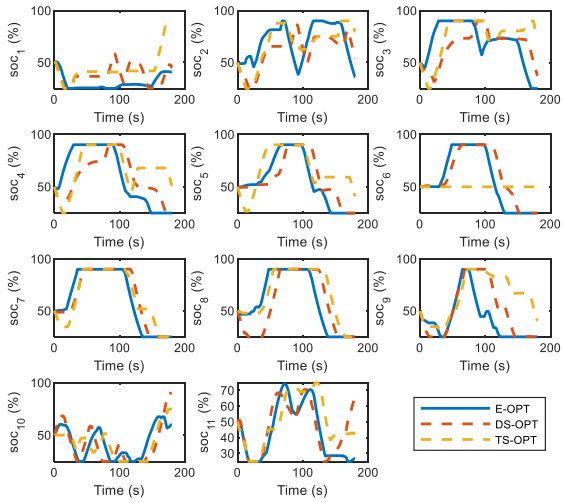

Fig. 32. The SOC curves of SCESSs along the metro line when $H = 180$ s.

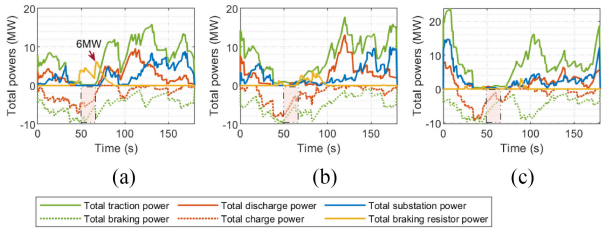

Fig. 33. The total operation powers when $H = 180$ s.

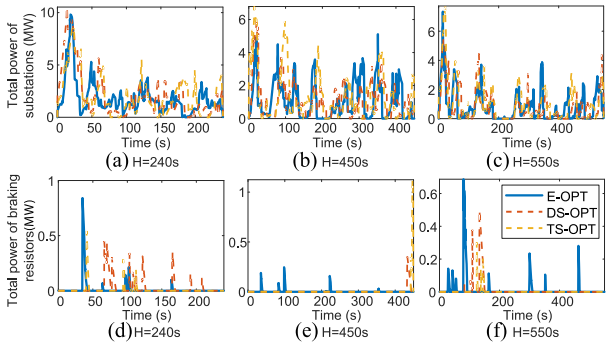

Fig. 34. The total operation powers of substations and braking resistors when $H = 240$ s, 450 s and 550 s.

hardly charged in the beginning, when the regenerative energy can be utilized by powering trains. And it's observed from Fig. 33(b) and (c) that the total braking power of trains during 50–70 s (when the total traction power of trains is small) is reduced by adjustment of train diagrams, and then increases later when more trains are powering, which improves the spatial and temporal distribution of regenerative energy. Though the SCESS configuration under TS-OPT is less than those under E-OPT and DS-OPT, the total power of braking resistors is reduced significantly. And it's also noticed that under TS-OPT, as no SCESS is installed in the 6-th station (Guanzhuang), the power of SCESS remains zero. Similarly, the total operation curves when $H = 240$ s, 450 s and 550 s are presented in Fig. 34. The intervention of braking resistors is significantly reduced than that of $H = 180$ s, and TS-OPT further reduces the total powers

TABLE IX
COMPARISON OF ENERGY CONSUMPTIONS FOR ALL-DAY OPTIMIZATION

Traffic conditions	E_{tot} (kWh)			E_{br} (kWh)		
	E-OPT	DS	TS	E-OPT	DS	TS
180s	176.2	161.1	146.2	34.8	17.4	4.8
240s	143.1	145.0	144.3	0.9	1.7	0.5
450s	143.7	143.5	144.8	0.4	0.6	1.3
550s	146.8	147.3	147.3	2.1	1.5	0.4
All-day	28595	28034	27586	1456.1	807.7	344.9

of braking resistors when $H = 240$ s and 550 s even with smaller SCESS configuration.

Table IX presents the total system energy consumption and braking resistor loss under the three optimization schemes. Compared with E-OPT, the synthetic optimization schemes reduce the ESS configuration capacity, while changes of energy consumption when the headways are 240 s, 450 s and 550 s are not obvious, and the braking resistors barely start, energy losses on braking resistors are within 2kWh. When the headway is 180 s, both the total energy consumption of the system and braking resistor loss are effectively reduced under the synthetic optimization scheme: they are 176.2 kWh and 34.8 kWh respectively under E-OPT, which means an amount of regenerative braking energy is still consumed by the braking resistors so as to achieve the trade-off between investment cost and energy-saving effect; however, under the TS-OPT, they are reduced to 146.2 kWh and 4.8 kWh respectively, the regenerative energy is recovered and utilized more effectively. The total system energy consumption for all-day under TS-OPT are reduced by 1009 kWh and 448 kWh respectively compared with E-OPT and DS-OPT, validating good energy-saving benefits of TS-OPT under all-day operating condition.

VII. CONCLUSION

In the traction power system with SCESSs, the parameters of trains, ESSs and power supply system interact with each other, and influence the energy efficiency of the system simultaneously. In this paper, the impact of each parameter on the energy transmission and consumptions is analyzed theoretically, and a two-stage multi-objective synthetic optimization algorithm for train diagrams, traction power parameters, and ESS capacity configuration is proposed. Based on simulation studies of Batong Line, the system parameters are optimmized under different headways and all-day operation scenario, the pareto curves under different optimization methods are obtained. The results show that the optimization of the trains' time-space distribution increases the regenerative braking energy transmission between trains; and by increasing the difference between the braking resistor's starting voltage and the substation no-load voltage, the intervention of braking resistors is delayed, and more regenerative energy is fed back to the power network. Therefore, compared with ESS-only optimization, the system energy consumption during whole-day is reduced by 1,009 kWh, while the ESS configuration cost is reduced by 8.68 million yuan under the proposed two-stage synthetic optimization, demonstrating that the SCESSs are utilized more effectively and good economic and energy-saving benefits are obtained.

In the future, this work will be further improved in three aspects: 1) Besides the utilization of regenerative braking energy, influences of the start voltage of braking resistors on the rail potential, system stability and regenerative failure will be analyzed and considered in the constraints of systematic optimization. 2) As SC also has the drawbacks of low energy density and high investment cost, we will make detailed economic analysis and comparison of different types of regenerative energy recovery technologies, and explore solutions with better economic and energy saving benefits, considering the rapid development of the energy storage technology in recent years. 3) In addition to the rule-based control strategy and static optimization in this paper, more advanced control algorithms, such as dynamic optimization and real-time adjustment with train states will be integrated in the synthetic optimization scheme to get better results.

REFERENCES

[1] D. U. S. Fabian Meishner, "Wayside energy recovery systems in DC urban railway grids," *eTransportation*, vol. 1, 2019, Art. no. 100001.

[2] T. Ratniyomchai, S. Hillmansen, and P. Tricoli, "Recent developments and applications of energy storage devices in electrified railways," *IET Elect. Syst. Transp.*, vol. 4, no. 1, pp. 9–20, 2013.

[3] S. Vazquez, S. M. Lukic, E. Galvan, L. G. Franquelo, and J. M. Carrasco, "Energy storage systems for transport and grid applications," *IEEE Trans. Ind. Electron.*, vol. 57, no. 12, pp. 3881–3895, Dec. 2010.

[4] H. Lee, J. Song, H. Lee, C. Lee, G. Jang, and G. Kim, "Capacity optimization of the supercapacitor energy storages on DC railway system using a railway powerflow algorithm," *Int. J. Innov. Comput., Inf. Control*, vol. 7, no. 5, pp. 2739–2753, 2011.

[5] R. Teymourfar *et al.*, "Stationary super-capacitor energy storage system to save regenerative braking energy in a metro line," *Energy Convers. Manage.*, vol. 56, pp. 206–214, 2012.

[6] R. Barrero, X. Tackoen, and J. Van Mierlo, "Improving energy efficiency in public transport: Stationary supercapacitor based energy storage systems for a metro network," in *Proc. Veh. Power Propulsion Conf.* 2008, pp. 1–8.

[7] C. H. Bae, "A simulation study of installation locations and capacity of regenerative absorption inverters in DC 1500 V electric railways system," *Simul. Modelling Pract. Theory*, vol. 17, no. 5, pp. 829–838, 2009.

[8] B. Wang, Z. Yang, F. Lin, and W. Zhao, "An improved genetic algorithm for optimal stationary energy storage system locating and sizing," *Energies*, vol. 7, no. 10, pp. 6434–6458, 2014.

[9] C. Wu, S. Lu, F. Xue, L. Jiang, and M. Chen, "Optimal sizing of onboard energy storage devices for electrified railway systems," *IEEE Trans. Transport. Electrific.*, vol. 6, no. 3, pp. 1301–1311, Sep. 2020.

[10] G. Graber, V. Calderaro, V. Galdi, A. Piccolo, R. Lamedica, and A. Ruvio, "Techno-economic sizing of auxiliary-battery-based substations in DC railway systems," *IEEE Trans. Transport. Electrific.*, vol. 4, no. 2, pp. 616–625, Jun. 2018.

[11] V. I. Herrera, H. Gaztañaga, A. Milo, A. Saez-de-Ibarra, I. Etxeberria-Otadui, and T. Nieva, "Optimal energy management and sizing of a battery-supercapacitor-based light rail vehicle with a multiobjective approach," *IEEE Trans. Ind. Appl.*, vol. 52, no. 4, pp. 3367–3377, Jul./Aug. 2016.

[12] G. Graber, V. Galdi, V. Calderaro, and A. Piccolo, "Sizing and energy management of on-board hybrid energy storage systems in urban rail transit," in *Proc. Int. Conf. Elect. Syst. Aircr., Railway, Ship Propulsion Road Veh. Int. Transp. Electrific. Conf.*, 2016, pp. 1–6.

[13] W. Yu, Y. Zhongping, and L. Feng, "Optimization of energy management strategy and sizing in hybrid storage system for tram," *Energies*, vol. 11, no. 4, 2018, Art. no. 752.

[14] A. González-Gil, R. Palacin, and P. Batty, "Sustainable urban rail systems: Strategies and technologies for optimal management of regenerative braking energy," *Energy Convers. Manage.*, vol. 75, pp. 374–388, 2013.

[15] A. J. López-López, R. R. Pecharromán, A. Fernández-Cardador, and A. P. Cucala, "Assessment of energy-saving techniques in direct-current-electrified mass transit systems," *Transp. Res. Part C: Emerg. Technol.*, vol. 38, pp. 85–100, 2014.

[16] M. Dominguez, A. Fernández-Cardador, A. P. Cucala, and R. R. Pecharroman, "Energy savings in metropolitan railway substations through regenerative energy recovery and optimal design of ato speed profiles," *IEEE Trans. Automat. Sci. Eng.*, vol. 9, no. 3, pp. 496–504, Jul. 2012.
[17] X. Yang, X. Li, B. Ning, and T. Tang, "A survey on energy-efficient train operation for urban rail transit," *IEEE Trans. Intell. Transp. Syst.*, vol. 17, no. 1, pp. 2–13, Jan. 2016.
[18] S. Su, X. Wang, Y. Cao, and J. Yin, "An energy-efficient train operation approach by integrating the metro timetabling and ECO-driving," *IEEE Trans. Intell. Transp. Syst.*, vol. 21, no. 10, pp. 4252–4268, Oct. 2020.
[19] F. Lin, S. Liu, Z. Yang, Y. Zhao, Z. Yang, and H. Sun, "Multi-train energy saving for maximum usage of regenerative energy by Dwell time optimization in urban rail transit using genetic algorithm," *Energies*, vol. 9, no. 3, 2016, Art. no. 208.
[20] M. Miyatake and H. Ko, "Optimization of train speed profile for minimum energy consumption," *IEEJ Trans. Elect. Electron. Eng.*, vol. 5, no. 3, pp. 263–269, 2010.
[21] P. Liu, L. Yang, Z. Gao, Y. Huang, S. Li, and Y. Gao, "Energy-efficient train timetable optimization in the subway system with energy storage devices," *IEEE Trans. Intell. Transp. Syst.*, vol. 19, no. 12, pp. 3947–3963, Dec. 2018.
[22] W. Kampeerawat and T. Koseki, "A strategy for utilization of regenerative energy in urban railway system by application of smart train scheduling and wayside energy storage system," *Energy Procedia*, vol. 138, pp. 795–800, 2017.
[23] W. Kampeerawar, T. Koseki, and F. Zhou, "Efficient urban railway design integrating train scheduling, onboard energy storage, and traction power management," in *Proc. Int. Power Electron. Conf.*, 2018, pp. 3257–3264.
[24] L. Chen, W. Hu, Q. Sun, J. Lv, and G. Zhao, "The influence of upper limit of network voltage on the train's regenerative braking energy utilization," *Electrified Railway*, no. 5, pp. 47–50, 2014.
[25] H. Xia, Z. Yang, Z. Yang, F. Lin, and X. Li, "Control strategy of supercapacitor energy storage system for urban rail transit based on operating status of trains," *Trans. China Electrotechnical Soc.*, vol. 32, no. 21, pp. 16–23, 2017.
[26] F. Zhu, Z. Yang, F. Lin, and Y. Xin, "Synthetic optimization of traction power parameters and energy storage systems in urban rail transit," *Diangong Jishu Xuebao/Trans. China Electrotechnical Soc.*, vol. 34, no. 3, pp. 579–588, 2019.
[27] J. Yang, "Electric traction system of metro vehicle for Beijing Batong line," *Electric Locomotives Mass Transit Veh.*, vol. 28, no. 5, pp. 8–11, Oct. 2005.
[28] A. Xu, "Research on regenerating energy utilization technique in urban rail system," Ph.D. dissertation, Nanjing Univ. Aeronaut. Astronaut., Oct. 2009.
[29] K. Zhao, "Energy management and capacity configuration of on-board EDLC energy storage system of railway vehicle," Ph.D. dissertation, Beijing Jiaotong Univ., Feb. 2013.
[30] J. Miller, *Ultracapacitor Applications*. Beijing, China: China Machine Press, 2014.
[31] F. Zhu, Z. Yang, F. Lin, and Y. Xin, "Decentralized cooperative control of multiple energy storage systems in urban railway based on multiagent deep reinforcement learning," *IEEE Trans. Power Electron.*, vol. 35, no. 9, pp. 9368–9379, Sep. 2020.
[32] T. Zhou and H. Zhang, *Electric Network Theory: Graph Theory, Equation, Synthesis*. Beijing, China: China Machine Press, 2008.
[33] K. Deb, *Multi-Objective Optimization Using Evolutionary Algorithms*. New York, NY, USA: Wiley, 2001.

Feiqin Zhu (Student Member, IEEE) received the B.S. and Ph.D. degrees in electrical engineering from Beijing Jiaotong University, Beijing, China, in 2015 and 2020, respectively.

She is currently a Postdoctor with the School of Vehicle and Mobility, Tsinghua University, Beijing, China. Her research interests include energy-saving technologies in urban railway and the PV-ESS-EV microgrid system.

Zhongping Yang (Member, IEEE) received the B.Eng. degree in electrical engineering from the Tokyo University of Mercantile Marine, Tokyo, Japan, in 1997, and the M.Eng. and Ph.D. degrees in electrical engineering from the University of Tokyo, Tokyo, Japan, in 1999 and 2002, respectively.

He is currently a Professor with the School of Electrical Engineering, Beijing Jiaotong University, Beijing, China. His research interests include high-speed rail integration technology, traction & regenerative braking technology, and wireless power transfer of urban rail vehicles.

He was the recipient of the Zhan Tianyou Award for Science and Technology in 2010, the Excellent Popular Science and Technology Book Award in 2011 and the Science and Technology Progress Award (second prize) of the Ministry of Education in China in 2016.

Ziwei Zhao received the B.S. degree in electrical engineering from Beijing Jiaotong University, Beijing, China, in 2019, where she is currently working toward the M.S. degree with the School of Electrical Engineering.

Her research interests include lithium-ion capacitors' modeling and tests, wayside and onboard energy storage system cooperative control, and energy management in urban rail transit.

Fei Lin (Member, IEEE) received the B.S. degree Xi'an Jiaotong University, Xi'an, China, in 1997, the M.S. degree from Shandong University, Jinan, China, in 2000, and the Ph.D. degree from Tsinghua University, Beijing, China, in 2004, all in electrical engineering.

He is currently a Professor with the School of Electrical Engineering, Beijing Jiaotong University, Beijing, China. His research interests include traction converter and motor drives, energy management for railway systems, and digital control of power-electronic-based devices.